Structural Determinants for the Differences in Voltage Gating of Chicken Cx56 and Cx45.6 Gap-Junctional Hemichannels

Jun-Jie Tong and Lisa Ebihara
Department of Physiology and Biophysics, Rosalind Franklin University of Medicine and Science, North Chicago, Illinois 60064

ABSTRACT The voltage- and calcium-dependent gating properties of two lens gap-junctional hemichannels were compared at the macroscopic and single channel level. In solutions containing zero added calcium and 1 mM Mg, chicken Cx56 hemichannels were mostly closed at negative potentials and application of depolarizing voltage clamp steps elicited a slowly activating outward current. In contrast, chicken Cx45.6 hemichannels were predominantly open at negative potentials and rapidly closed in response to application of large depolarizing potentials. Another difference was that macroscopic Cx45.6 currents were much smaller in size than the hemichannel currents induced by oocytes with similar amounts of cRNA for Cx56. The aim of this study was to identify which regions of the connexins were responsible for the differences in voltage-dependent gating and macroscopic current amplitude by constructing a series of chimeric Cx45.6-Cx56 channels. Our results show that two charged amino acids that are specific for the α3-group connexins (R9 in the N-terminus and E43 in the first extracellular loop) are important determinants for the difference in voltage-dependent gating between Cx45.6 and Cx56 hemichannels; the first transmembrane-spanning domain, M1, is an important determinant of macroscopic current magnitude; R9 and E43 are also determinants of single channel conductance and rectification.

INTRODUCTION

Connexons or gap junctional hemichannels are large, relatively nonselective ion channels that reside in the nonjunctional plasma membrane at least transiently before their assembly into gap junctional channels. It was originally thought that unpaired hemichannels must remain closed for a cell to maintain a normal resting potential and proper transmembrane ionic gradients. However, there have been a number of recent studies that suggest that these channels can open under certain conditions such as ischemia (1,2) or mechanical strain (3) and may participate in a number of cellular processes including the release of small metabolites, such as ATP, which are involved in paracrine signaling (4–7). Connexons are composed of six subunits called connexins. The connexins belong to a multigene family composed of at least 20 human members (8). All of the connexins have four membrane-spanning domains, and both the NH_2- and COOH-termini reside on the cytoplasmic side of the membrane.

A common feature of most connexons is that they are blocked by external divalent cations and hyperpolarized transmembrane potentials (9–13). These two effects act synergistically to prevent the opening of unpaired hemichannels under normal physiological conditions. However, within the connexin family, there are significant differences in voltage gating properties and divalent cation sensitivity. In addition, these channels exhibit differences in single channel conductance and rectification.

In this study, we focus on the voltage gating properties of two prototypic connexins. These are chicken Cx56 and chicken Cx45.6, both of which are coexpressed in lens fiber cells.

MATERIALS AND METHODS

Construction of chimeric and mutant subunits

We constructed eight chimeric constructs in which one or more domains and/or amino acids of Cx45.6 were replaced by the corresponding domains and/or amino acids of Cx56 using polymerase chain reaction (PCR) amplification. In addition, we constructed one chimeric construct in which two amino acids of Cx56 were replaced by the corresponding amino acids of Cx45.6. The domains of the two connexins are delimited as follows. Cx56 is divided into N (Metl-Lys-23), M1 (Val-24-Ala-41), E1 (Glu-42-Arg-76). Cx45.6 is divided into N (Met-l-Arg-23), M1 (Val-24-Ala-41), E1 (Glu-42-Arg-76). Generation of Cx45.6-56N and Cx45.6-56M1 constructs are described in Tong et al. (18). Cx45.6-56NM1, Cx45.6L43E-56M1, Cx45.6N9R-56M1, Cx45.6N9RL43E-56M1, Cx45.6R9N-56NM1, and Cx56R9NE43L were constructed using the QuikChange Site-Directed Mutagenesis kit (Stratagene, La Jolla, CA) according to the manufacturer's protocol. All of the constructs were sequenced (DNA Sequencing and Synthesis Facility, Iowa State University, Ames, IA) to ensure that PCR amplification did not introduce random mutations.

Expression of connexins in *Xenopus* oocytes

Adult female *Xenopus laevis* frogs were anesthetized on ice and a partial ovarectomy performed. The oocytes were defolliculated by treating them with collagenase IA (Sigma Chemical, St. Louis, MO). Stage V and VI oocytes were selected and pressure injected using a Nanoject variable microinjection apparatus (model No. 3-000-203, Drummond Scientific, Broomal, PA) with 0.23 ng of oligonucleotides antisense to mRNA for *Xenopus* Cx38 as previously described (14). The oocytes were incubated overnight at 18°C in Modified Barth's Solution (MBS) containing (in mM) 88 NaCl, 1 KCl, 2.4 $NaHCO_3$, 15 Hepes, .3 $CaNO_3$*$4H_2O$, 0.41

Submitted February 6, 2006, and accepted for publication June 2, 2006.

Address reprint requests to Lisa Ebihara, Dept. of Physiology and Biophysics, Rosalind Franklin School of Medicine and Science/Chicago Medical School, 3333 Green Bay Rd. North, Chicago, IL 60064. Tel.: 847-578-3424; Fax: 847-578-3265; E-mail: lisa.ebihara@rosalindfranklin.edu.

0006-3495/06/09/2142/13 $2.00

doi: 10.1529/biophysj.106.082859

$CaCl_2$*$6H_2O$, 0.82 $MgSO_4$*H_2O, 550 mg/L pyruvate, and 50 μg/ml gentamycin, pH 7.4. Connexin cRNAs were synthesized using the mMessage mMachine in vitro transcription kit (Ambion, Austin, TX) according to the manufacture's instructions. The amount of cRNA was quantitated by measuring the absorbance at 260 nm. The purity and amount of cRNA was further assessed by agarose gel electrophoresis. Cx38 antisense-pretreated oocytes were injected with 36 nl of 0.04-4 ng/nl connexin cRNA and incubated for an additional 16–24 h at 18°C in MBS containing 5 mM $CaCl_2$.

Electrophysiological measurement and analysis of hemi-gap-junctional channels expressed in *Xenopus* oocytes

Voltage clamp recordings of macroscopic hemichannel currents from single oocytes were obtained with a two-microelectrode-voltage-clamp (Gene clamp 500, Axon Instruments, Foster City, CA). The microelectrodes were filled with 3 M KCl and had resistances between 0.1 and 1.0 MΩ. To prevent electrode leakage, the tips of the electrodes were backfilled with 1% agar in 3 M KCl. The standard external bath solution contained (in mM) 88 choline chloride, 1.0 KCl, 2.4 $NaHCO_3$, 1.0 $MgCl_2$, and 15 Hepes, pH 7.6. Choline was used instead of sodium in the bath solution to prevent the inward flow of current through endogenous sodium channels at potentials $\geq +40$ mV.

For the dose-response curves for calcium blockade, connexin cRNA-injected oocytes were thoroughly washed in the choline chloride solutions containing different calcium concentrations. No calcium buffer was used for solutions containing $\geq 10^{-5}$ M free Ca^{2+}. A total of 1 mM EGTA and 0.5 mM Ca^{2+} was added to the solution intended to contain 0.026 μM $[Ca^{2+}]_o$. The amplitude of the current at the end of a 2.5-s pulse to -50 mV from a holding potential -10 mV was measured, and the concentration-response curve showing inhibition of hemichannel current at as a function of $[Ca^{2+}]$ was determined. Block was assumed to be absent in solutions containing 0.026 μM $[Ca^{2+}]_o$. The data were corrected for leakage by subtracting the average leakage current measured in control oocytes (oocytes injected only with AS). All experimental data presented are averages from five to nine oocytes from the same donor. The experiments were repeated with a different donor to verify the reproducibility of the basic findings. The concentration-response relationships were fit with Langmuir isotherms of the form $\%Block = A/(1 + 10^{(\log(IC50) - [M])p})$, where A is maximum response (normalized to 1 for Ca^{2+}), IC_{50} is the half-maximal inhibitory concentration, [M] is the concentration of the metal ion, and p is the Hill coefficient.

The conductance-voltage curves were determined from isochronal tail currents. The membrane potential was stepped from -10 mV to the test potential for 20 s and then hyperpolarized to -80 mV. Tail current amplitudes were determined at 10–12 ms after repolarization. The amplitudes were corrected by subtracting the leakage current estimated from control oocytes (oocytes injected only with AS). The tail currents were then normalized to the tail current amplitude after a 20 mV or 40 mV test pulse and plotted as a function of test potential. The voltage dependence of activation was quantified by fitting the curves to a Boltzmann function ($I = a/(1+\exp((V - V_{0.5})/b))$) using SigmaPlot 8.0 software (SPSS, Chicago, IL). For this analysis, the relative probability of opening was assumed to approach zero at large negative potentials. The time course of deactivation was obtained by fitting decaying tail currents to a biexponential function.

All experiments were performed at room temperature (20–24°C). Pulse generation and data acquisition were performed using a PC computer equipped with PCLAMP 6 software and a TL-1 acquisition system (Axon Instruments). Currents were filtered at 50–100 Hz and digitized using PCLAMP6 software and a Digidata 1200 interface (Axon Instruments). Leak correction, when applied, was performed by extrapolating from linear regression to data at negative potentials or by subtracting the average leakage current in control oocytes (oocytes injected only with AS); and ~8–10 ms at the beginning of each step was blanked.

For single channel measurements, the oocyte vitelline membrane was removed (15) and the channels were studied with the patch-clamp technique. All measurements were performed at room temperature. Pipettes were pulled using a Flamming/Brown micropipette puller (model P-87; Sutter Instruments, Novato, CA). The patch pipettes had resistances of 2–5 MΩ when filled with standard internal solution containing (in mM) 140 KCl, 1 EGTA, .5 $CaCl_2$, 1 $MgCl_2$, 5 Hepes, pH 7.6. The bath chamber contained the same solution as the pipettes. Single channel currents were recorded in the cell-attached patch configuration using an Axopatch 200B amplifier (Axon Instruments). Signals were filtered at 1 kHz and digitized with a Digidata 1322A analog/digital converter (Axon Instruments) at 10 kHz, unless otherwise noted, using pClamp 9.2 (Axon Instruments). Single channel I-V curves were determined using 200-ms voltage clamp ramps between -100 mV and 100 mV. The I-V curves of the main open state were constructed by subtracting a segmented average trace of the baseline current from a single current trace or a segmented average trace of the current when the channel was in the main open state.

Data analysis was performed using PCLAMP 9.2 software (Axon Instruments), Microcal Origin Version 7 (OriginLab, Northhampton, MA), and SigmaPlot Version 8.0 (SPSS). Group statistics were reported as mean ± SE.

All chemicals were obtained from Sigma-Aldrich.

RESULTS

Fig. 1 compares representative families of calcium-sensitive currents and I-V curves recorded from single oocytes injected with *Xenopus* Cx38 antisense oligonucleotides alone or antisense + cRNA for Cx56 or Cx45.6. Although both Cx56 and Cx45.6 cRNA-injected oocytes develop calcium-sensitive currents, their voltage gating properties (in choline chloride solution containing zero added calcium and 1 mM Mg^{+2}) show marked differences.

Cx45.6 channels resided primarily in the open state at a holding potential of -10 mV and tended to close at large positive and negative potentials (Fig. 1 *A*). The rate and extent of channel closure was much greater at large positive potentials (inactivation) compared to negative potentials (deactivation). Repolarization to -80 mV after a depolarizing test pulse to $+60$ or $+80$ mV induced a hooked tail current (Fig. 1 *A*, *inset*). The hook in the tail current most likely represents rapid recovery from channel inactivation that occurred during the preceding test pulse.

In contrast, Cx56 channels had a substantial probability of being in the closed state at a holding potential of -10 mV. Application of depolarizing voltage clamp steps elicited an instantaneous jump in current followed by a slowly activating outward current (Fig. 1 *B*). Repolarization to -80 mV after a depolarizing test pulse induced a tail current that decayed monotonically to zero. The rates of current deactivation were much faster than those of Cx45.6. Another difference was that the Cx56 hemichannel currents were considerably larger in size than macroscopic hemichannel currents induced by injecting oocytes with similar amounts of cRNA for Cx45.6. These results are very similar to those reported earlier for rat Cx46 (the rat ortholog of Cx56) and mouse Cx50 (the mouse ortholog of Cx45.6) (16,17). However, unlike mouse Cx50, the amplitude of the

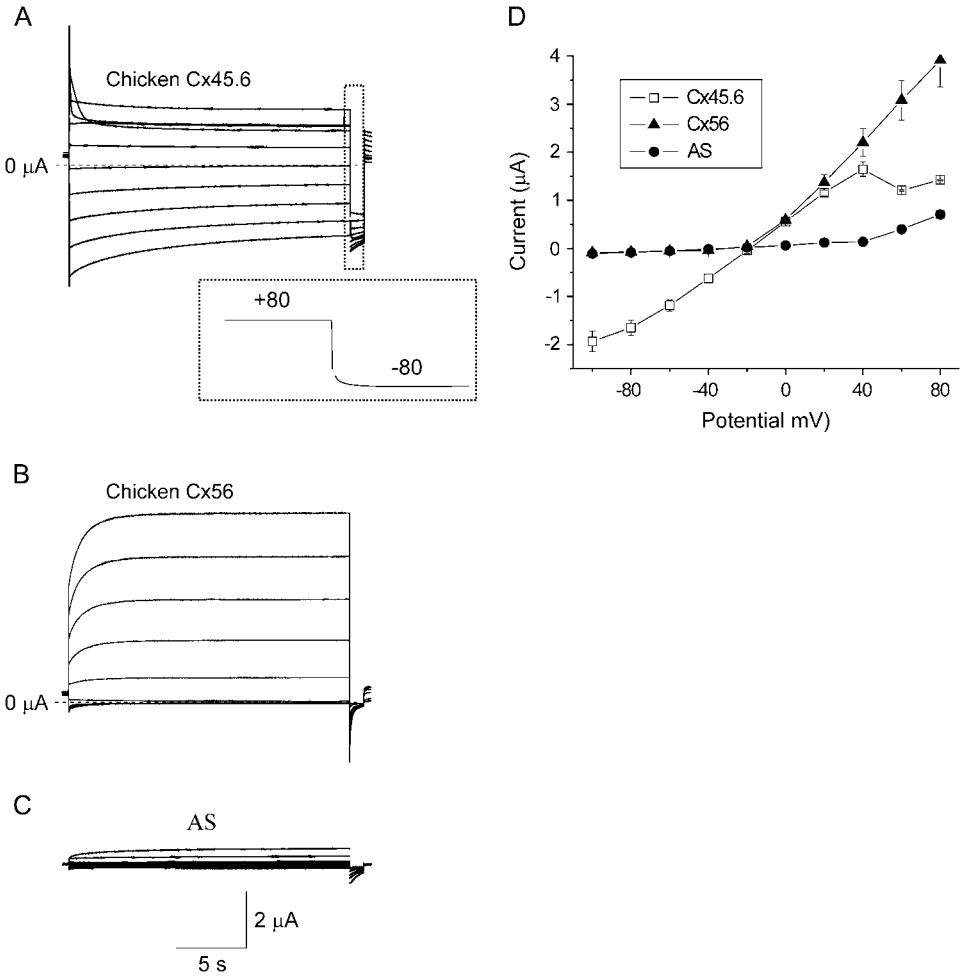

FIGURE 1 Hemichannel currents composed of chicken Cx56 and chicken Cx45.6 exhibit distinct voltage-dependent properties. (*A*) Representative families of current traces recorded from single oocytes injected with *Xenopus* Cx38 antisense oligonucleotides + cRNA for Cx45.6 (*A*), Cx56 (*B*), or antisense oligonucleotides alone (*C*) in zero Ca^{2+} choline chloride solution. Inset in panel *A* shows tail current on an expanded timescale; test potential = +80 mV. The oocytes were held at −10 mV between pulse sequences to minimize holding currents. A 20-s test pulse was applied to voltages between +80 mV and −100 mV in decrements of 20 mV followed by a shorter pulse to −80 mV. No leakage current correction. Dashed line represents zero current. (*D*) Quasi-steady-state I-V relationships for Cx56 (*solid triangles*, $n = 4$), Cx45.6 (*open squares*, $n = 4$), and AS alone (*solid circles*, $n = 5$) were determined by measuring the current at the end of the test pulse and plotting it as a function of pulse potential.

Cx45.6-induced currents was insensitive to changes in external pH between 6.6 and 8.6 (data not shown).

The properties of Cx45.6 and Cx56 were also examined at the single channel level. Fig. 2 shows representative single channel current traces, ensemble averages, and single channel I-V curves recorded from Cx45.6 or Cx56 cRNA-injected oocytes using the cell attached patch clamp technique with $\sim 10^{-9}$ $[Ca^{2+}]_o$ and 1 mM $[Mg^{2+}]_o$ in the pipette solution. The gating properties of Cx45.6 hemichannels were very different from those of Cx56. Cx45.6 hemichannels closed on depolarization to +40 mV and opened on hyperpolarization to −40 mV. In contrast, Cx56 hemichannels opened on depolarization and closed on hyperpolarization. Ensemble averages of single Cx45.6 and Cx56 hemichannels resembled records of the corresponding macroscopic currents from whole oocytes. The two types of hemichannels also showed differences in single channel conductance (see Table 2). The single channel I-V curve of Cx45.6 was linear and had a slope conductance of 536.5 ± 37.3 pS ($n = 4$). In contrast, the single channel I-V curve of Cx56 rectified inwardly and had a slope conductance of 355.8 ± 15.02 pS ($n = 6$) at 0 mV. These values are similar to those reported for Cx50 and Cx46 (17).

Role of the first transmembrane-spanning domain, M1

To identify the Cx56 sequences responsible for these differences, several chimeras and reciprocal point mutations between Cx45.6 and Cx56 were examined (Fig. 3). We initially focused on the first transmembrane-spanning domain (M1) because our previous work had shown that expression of a Cx45.6 chimera containing the first transmembrane domain of Cx56 (Cx45.6-56M1) caused the oocytes to develop a large membrane conductance that could not be prevented by incubation in 2 mM $[Ca^{2+}]_o$ (18).

Expression of Cx45.6-56M1 in oocytes produced hemichannel currents that were much larger than wild-type Cx45.6 (when studied under identical conditions in oocytes injected with similar amounts of cRNA). The current was so large that in many cells, we were unable to accurately measure it, especially in the presence of reduced $[Ca^{2+}]_o$. To reduce the size of the current, oocytes were injected with 50–200-fold less cRNA than that used to express wild-type Cx45.6. Fig. 4 *A* shows a representative family of current traces recorded during voltage clamp steps from a holding

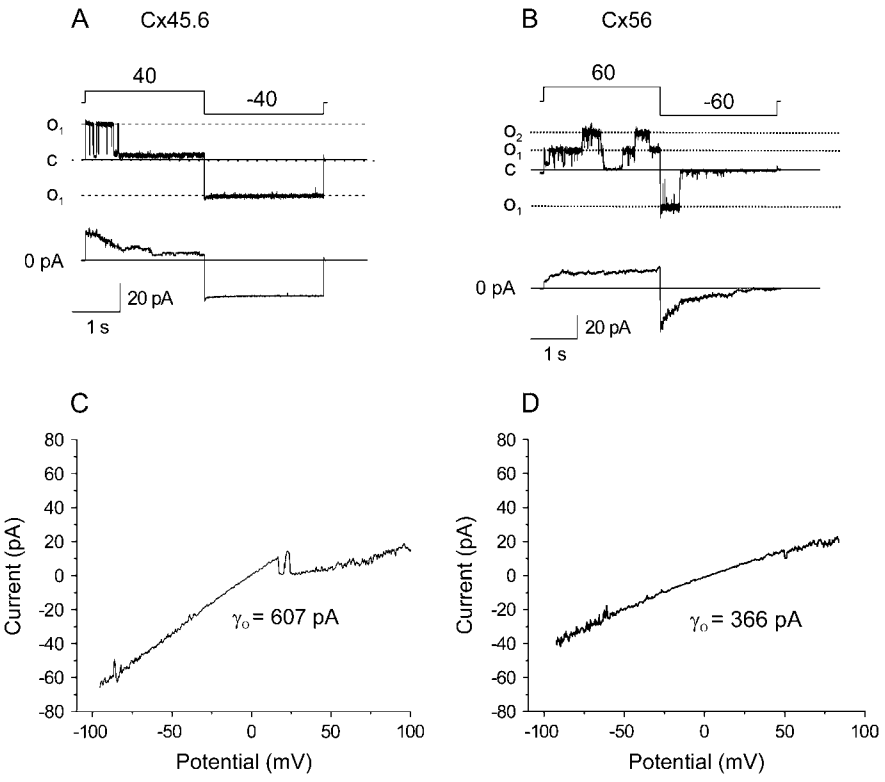

FIGURE 2 Single channel current traces of Cx45.6 and Cx56 in the cell-attached mode. The pipette solution contained (in mM) 140 KCl, .5 Ca^{2+}, 1 Mg^{2+}, 1 EGTA. (*A*) Upper panel shows a record of a single Cx45.6 channel for voltage clamp steps of ±40 from a holding potential of 0 mV. Lower panel shows the average of 14 such records. The channels were predominantly in the open state at 0 mV and then closed to a long-lasting substate after application of a voltage clamp step to +40 mV. When the potential was changed to −40 mV, the channel reopened and remained in the fully open state for duration of the pulse. (*B*) Upper panel shows a record of two Cx56 channels for voltage clamp steps of ±60 from a holding potential of 0 mV. Lower panel shows ensemble average of 21 such records. When the potential was held at 0 mV, the channel was rarely open, but at +60 mV, the channels opened. When the potential was suddenly stepped from +60 to −60 mV, the channel was initially open and then closed to the fully closed state. Data corrected for leakage by subtracting a segmented average trace of the baseline current. (*C* and *D*) Current-voltage relationships for Cx45.6 (*C*) and Cx56 (*D*) obtained by application of a 200-ms voltage ramp between ±100 mV to cell-attached patches containing only one active channel. The Cx45.6 channel shown in panel *C* closed from the main open state to a long-lasting substate at positive potentials. Corrected for leakage current as described in Materials and Methods.

potential of −10 mV in zero calcium solution. The voltage gating properties of Cx45.6-56M1 were similar to those of wild-type Cx45.6 except that the Cx45.6-56M1 current exhibited a more prominent decline at large negative potentials (Fig. 4 *B*).

One explanation for the enhanced size of Cx45.6-56M1 compared to wild-type Cx45.6 was that Cx45.6-56M1 was less sensitive to block by external calcium. To test this hypothesis in a quantitative manner, the inhibition of the currents at a holding potential of −10 mV was plotted as a function of $[Ca^{2+}]_o$ and fitted to the equation:

$$\%Block = 100/(1 + 10^{(\log(IC50) - [Ca^{2+}])p}),$$

where IC_{50} is the half-maximal inhibitory concentration and p is the Hill coefficient (Fig. 4 *C*). The IC_{50} for Cx45.6-56M1 was .68 mM with a Hill coefficient of 1.53. The IC_{50} for Cx45.6 was .012 mM with a Hill coefficient of 0.81. The effects of removal of external calcium on the magnitude of the current were completely reversible upon addition of calcium to the bathing solution (data not shown).

Cx45.6-56NM1 channels close at negative potentials

Another domain that plays a critical role in hemichannel gating is the N-terminus (N). Expression of a Cx45.6 chimera containing both the N-terminus and the first transmembrane domain of Cx56 (Cx45.6-56NM1) resulted in the development of large hemichannel currents whose magnitude was comparable to Cx45.6-56M1. However, in contrast to Cx45.6-56M1, Cx45.6-56NM1 channels were mostly open at positive potentials and rapidly closed when the membrane potential was changed to negative potentials as illustrated in Fig. 5 *A*. The steady-state current magnitude of Cx45.6-56NM1 was markedly reduced at potentials negative to −10 mV compared to Cx45.6-56M1 (Fig. 5 *B*). Fig. 5 *C* compares the time course of deactivation of Cx45.6-56M1 and Cx45.6-56NM1 at −100 mV to demonstrate the striking difference in deactivation kinetics of these two chimeras. Fig. 5 *D* compares the isochronal conductance-voltage curves for Cx45.6-56NM1 and Cx45.6-56M1 determined by plotting the relative amplitude of the tail current at −80 mV as a function of test potential. The currents were normalized to the tail current measured after a pulse to +20 mV. The voltage dependence of activation was quantified by fitting the curves to a Boltzmann function (Table 1). The $V_{0.5}$ was −50.2 mV and the slope factor was 12.52 mV for Cx45.6-56NM1 compared with a $V_{0.5}$ of −78.9 mV and a slope factor of 30 mV for Cx45.6-56M1.

Cx45.6-56NM1 and Cx45.6-56M1 also showed differences in inactivation kinetics at large positive potentials. The time course of inactivation of Cx45.6-56NM1 was consistently slower than that of Cx45.6-56M1 at +80 mV. Unfortunately, the inactivation properties of the different

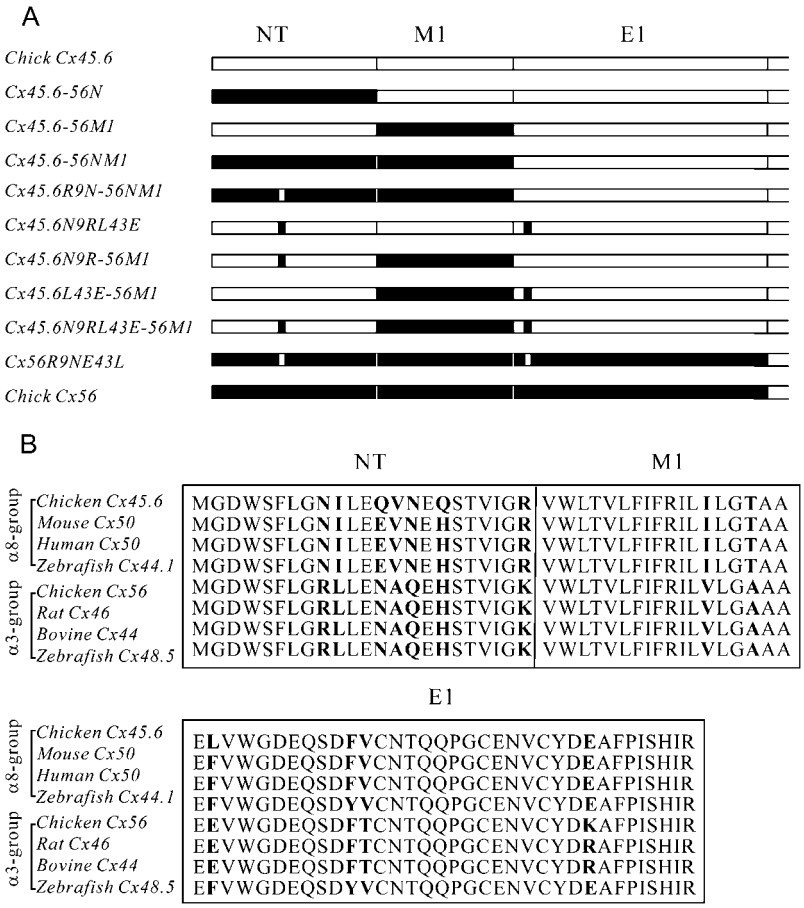

FIGURE 3 (*A*) Schematic representation of chimeric connexins made by swapping domains between Cx45.6 (*open*) and Cx56 (*solid*). (*B*) Amino acid sequence alignment of the N-terminal, M1, and E1 domains of the α8- and α3-group connexins.

constructs were frequently partially masked by current activation and by contamination of the exogenous currents by endogenous outward sodium currents at potentials greater than 40 mV. Therefore no attempt was made to quantify these differences in inactivation properties.

It was previously shown that a uniquely occurring arginine at residue 9 in the N-terminus of the α3-group connexins is the main determinant for the differences in voltage-dependent gating properties between Cx46 (the rat ortholog of Cx56) and Cx45.6 gap junctional channels (18). Thus we were interested in examining the role of this amino acid in hemichannel gating. Our results show that when N9 of Cx45.6-56M1 was mutated to arginine (the positively charged α3-specific amino acid in the N-terminus) or lysine (data not shown), the effect on channel function was the same as that of swapping the N-terminus: the channel rapidly closed at negative potentials and opened upon depolarization (Fig. 6 *A*). Comparison of the isochronal conductance-voltage curves of Cx45.6N9R-56M1 and Cx45.6-56NM1 showed that the two curves were very similar (Fig. 6 *B*; Table 1). These results suggest that the positive charge at residue 9 in the N-terminus of Cx56 plays an essential role in determining this behavior.

To further confirm the importance of a positive charged residue at position 9, we substituted an uncharged asparagine (the Cx45.6-specific amino acid) at this position in Cx45.6-56NM1 and demonstrated that this converted the biophysical properties of the resulting mutant channel back to those of Cx45.6-56M1 (Fig. 6, *C* and *D*).

Role of E43 in Ca^{2+} modulation of hemichannel gating

The position corresponding to E43 in the first extracellular loop of Cx56 is conserved among most of the α3-group connexins. Leucine is found in the analogous position in Cx45.6. To determine the contribution of E43 to hemichannel gating, three chimeric constructs were generated: Cx45.6L43E-Cx56M1, Cx45.6N9RL43E-Cx56M1, and Cx45.6N9RL43E. Fig. 7 shows representative families of macroscopic current traces and I-V curves for each of these constructs in the presence of zero added calcium. The biophysical properties of Cx45.6L43E-56M1 (Fig. 7 *A*) were most similar to Cx45.6-56M1. However, the isochronal conductance-voltage curve of Cx45.6L43E-56M1 was shifted to more depolarized potentials compared to Cx45.6-56M1 (Fig. 7 *D*; Table 1).

In contrast, Cx45.6N9RL43E-56M1 channels showed a remarkable resemblance to wild-type chicken Cx56 (Fig. 7 *B*). Both Cx45.6N9RL43E-56M1 and Cx56 were characterized

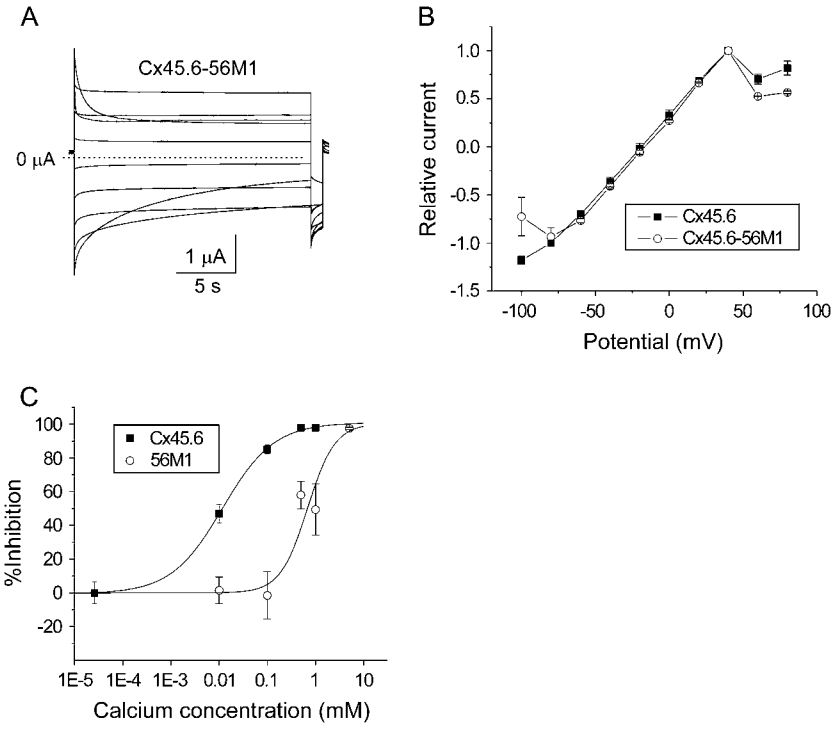

FIGURE 4 Properties of Cx45.6-56M1 hemichannel currents. (*A*) Representative current traces recorded in zero added calcium solution. Cx45.6-56M1 hemichannel currents were recorded in response to a series of 20-s voltage clamp steps from +80 mV to −100 mV in decrements of 20 mV followed by a short pulse to −80 mV. Holding potential = −10 mV. No leakage current correction. Dashed line represents zero current. The oocyte was injected with 50–200-fold less cRNA than that used to express wild-type Cx45.6 to reduce the size of the current. (*B*) Quasi-steady-state current-voltage curves recorded for Cx45.6 (*solid squares*, $n = 3$) and Cx45.6-56M1 (*open circles*, $n = 3$). (*C*) Concentration-response curves showing inhibition of Cx45.6 (*solid squares*) and Cx45.6-56M1 (*open circles*) as a function of $[Ca^{2+}]_o$. The IC_{50} for Cx45.6 was 0.012 mM with a Hill coefficient of 0.81. The IC_{50} for Cx45.6-56M1 was .68 mM with a Hill coefficient of 1.53.

by large outward currents that slowly activated in response to depolarizing pulses and relatively small inward currents that rapidly deactivated in response to hyperpolarization. The isochronal conductance-voltage curve of Cx45.6N9RL43E-56M1 was indistinguishable from that of chicken Cx56 (Fig. 7 *E*).

The effect of 56M1 on gating of Cx45.6N9RL43E-56M1 is illustrated in Fig. 7 *C*, which shows the corresponding construct without 56M1. No obvious changes in voltage-dependent gating properties were observed. The isochronal conductance-voltage curve of Cx45.6N9RL43E was identical to that of Cx45.6N9RL43E-56M1 (Fig. 7 *E*).

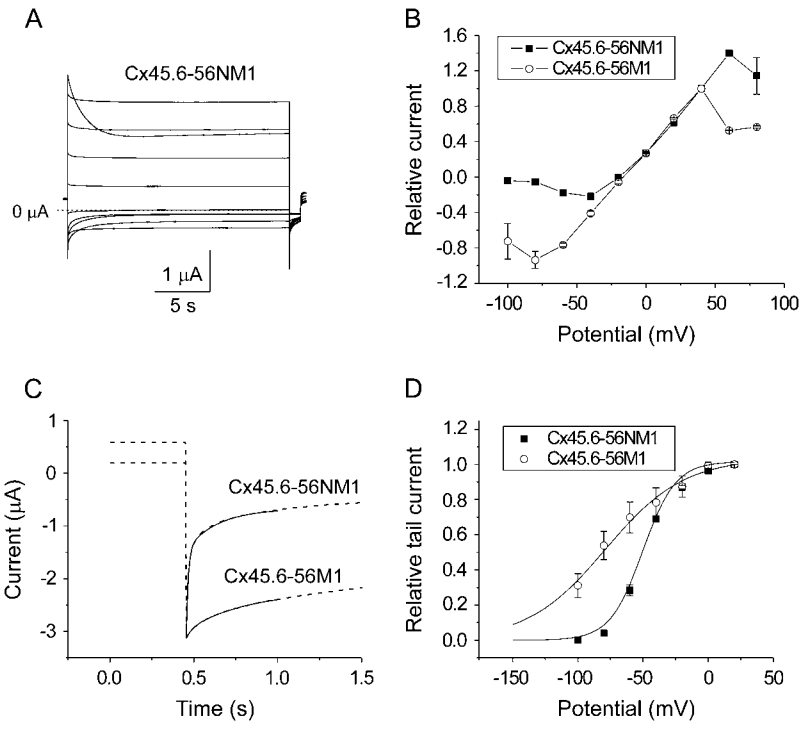

FIGURE 5 Cx45.6-56NM1 hemichannel currents rapidly close in response to hyperpolarizing voltage clamp steps. (*A*) Representative current traces recorded in zero added calcium solution. Cx45.6-56NM1 hemichannel currents were recorded in response to a series of 20-s voltage clamp steps from +80 mV to −100 mV in decrements of 20 mV followed by a short pulse to −80 mV. Holding potential = −10 mV. No leakage current correction. Dashed line represents zero current. (*B*) Quasi-steady-state current-voltage curves recorded for Cx45.6-56NM1 (*solid squares*, $n = 3$) and Cx45.6-56M1 (*open circles*, $n = 3$). The amplitude of the steady-state current was normalized with respect to the amplitude of the current at 40 mV. (*C*) Comparison of the time course of deactivation of Cx45.6-56NM1 and Cx45.6-56M1 currents on repolarization to −100 mV. Fits to a biexponential function (*solid lines*) are shown superimposed on the ionic current traces (*dashed lines*). For Cx45.6-56NM1, $\tau_{fast} = 11.9$ ms and $\tau_{slow} = 187.2$ ms. For Cx45.6-56M1, $\tau_{fast} = 37.6$ ms and $\tau_{slow} = 402.9$ ms. The tail currents have been normalized with respect to the peak tail current. (*D*) Isochronal conductance-voltage relationships for Cx45.6-56NM1 (*solid squares*, $n = 3$) and Cx45.6-56M1 (*open circles*, $n = 4$). Amplitude of tail currents were measured at −80 mV after 20-s pulses to different test potentials and then normalized to the amplitude of the tail current after a test pulse to +20 mV. Solid lines are the best fit of the G-V curves to a Boltzmann function whose parameters are given in Table 1.

TABLE 1 Voltage dependence of activation of wild-type and mutant connexins

Cx*	Threshold (mV)	$V_{0.5}$ (mV)	Slope factor (mV)
Cx45.6	N.D.	N.D.	N.D.
Cx56	−20	N.D.	N.D.
Cx45.6-56M1	N.D.	−79	30
Cx45.6-56NM1	−80	−50.2	12.5
Cx45.6N9R-56M1	−80	−48.3	10.3
Cx45.6-56NMIR9N	N.D.	−79.1	21.7
Cx45.6L43E-56M1	N.D.	−16.7	36.8
Cx45.6N9RL43E-56M1	−20	N.D.	N.D.
Cx56R9NE43L	N.D.	−71.25	24.6

N.D. unable to accurately determine activation parameters.
*Bath solution contained 0 added $[Ca^{2+}]_o$ and 1 mM $[Mg^{2+}]_o$.

These results are consistent with the hypothesis that M1 has little or no effect on voltage gating.

To compare the activation and deactivation kinetics of Cx45.6N9R-56M1, Cx45.6L43E-56M1, Cx45.6N9RL43E-56M1, and wild-type Cx56, the membrane was held at −80 mV to close the channels and a series of depolarizing voltage clamp steps ranging between −70 and 30 mV was applied (Fig. 8 *A*). The time course of activation of Cx45.6N9R-56M1 was faster than that of Cx45.6L43E-56M1, Cx45.6N9RL43E-56M1, or Cx56. This effect was quantified by measuring the time required to reach half peak current amplitude at +30 mV. The time to half peak current amplitude of Cx45.6N9R-56M1 was significantly smaller than that of Cx45.6L43E-56M1, Cx45.6N9RL43E-56M1, or Cx56 (Fig. 8 *B*). In contrast, the time to half peak current amplitude of Cx45.6L43E-56M1, Cx45.6N9RL43E-56M1, and Cx56 were not significantly different. Deactivating currents were best fit with a biexponential function. These results suggest that the rate of channel closure could be ranked in the following order: Cx45.6L43E-56M1 < Cx45.6N9R-56M1 < Cx45.6N9RL43E-56M1 ≅ Cx56 (Fig. 8, *C* and *D*).

We also examined the effect of the reciprocal mutations (R9N and E43L) on the voltage gating properties of chicken Cx56 hemichannel currents as illustrated in Fig. 9. Cx56R9NE43L channels were most similar to Cx45.6-56M1. Both Cx56R9NE43L and Cx45.6-56M1 exhibited a substantial open probability at hyperpolarized potentials and slow deactivation kinetics (Fig. 9 *A*). The isochronal conductance-voltage curve of Cx56R9NE43L resembled that of Cx45.6-56M1 (Fig. 9 *C*). Fig. 9 *B* compares the time course of deactivation of Cx56R9NE43L and Cx45.6-56M1 in response to a hyperpolarizing step to −100 mV to more clearly demonstrate the similarity in deactivation kinetics.

To further investigate the role of the negatively charged glutamic acid at position 43 in mediating the hyperpolarization-induced closing of Cx45.6L43E-56M1 and Cx45.6N9RL43E-56M1 channels, we examined the effects of removing external magnesium on gating (Fig. 10). In the absence of external Mg^{2+}, Cx45.6L43E-56M1 channels did not close at a holding potential of −80 mV and the quasi-steady-state I-V relationship exhibited mild outward rectification. The slow relaxation in response to voltage clamp steps that was observed in this record resembled that for the septal membranes of the median giant axon of the

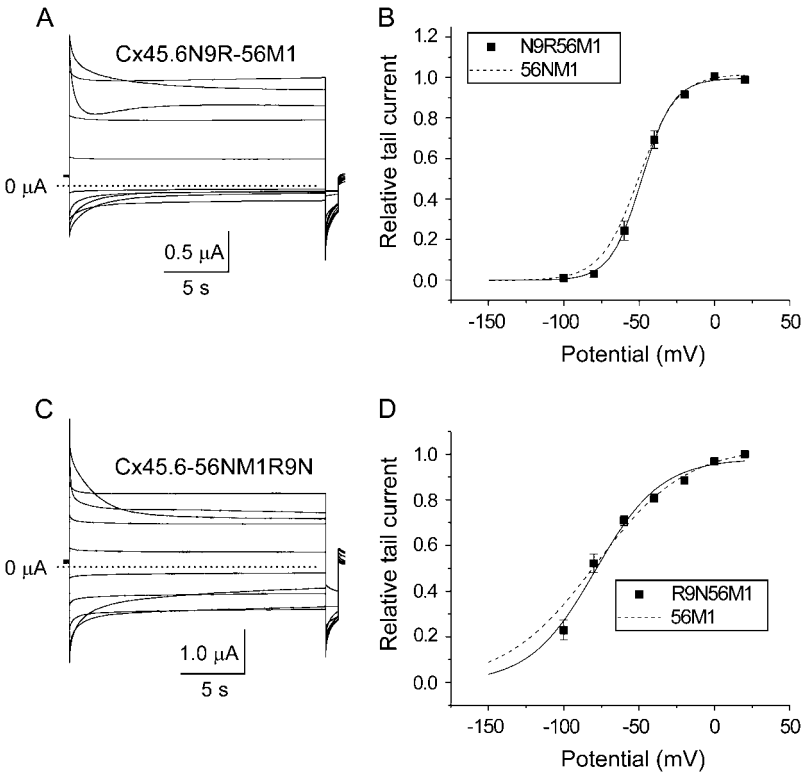

FIGURE 6 Cx45.6N9R-56M1 channels have voltage gating properties that resemble Cx45.6-56NM1. (*A*) Representative families of current traces recorded from oocytes expressing Cx45.6N9R-56M1 in response to voltage clamp steps from a holding potential of −10 mV to potentials ranging from +80 to −100 mV in −20-mV decrements followed by a short hyperpolarizing pulse to −80 mV in the presence of zero added calcium. No leakage current correction. Dashed line represents zero current. (*B*) Isochronal conductance-voltage curve for Cx45.6N9R-56M1 (*solid squares*, $n = 4$). The solid line is the best fit of the G-V curve to a Boltzmann function whose parameters are given in Table 1. For comparison, the fit of the data for Cx45.6-56NM1 (*dashed line*) is shown. (*C*) Cx45.6-56NM1R9N currents recorded in zero added calcium-containing solution. No leakage current correction. Dashed line represents zero current. Pulse protocol same as in panel *A*. (*D*) Isochronal conductance-voltage curve for Cx45.6-56NM1R9N (*solid squares*, $n = 5$). The solid line is the best fit of the G-V curves to a Boltzmann function whose parameters are given in Table 1. For comparison, the fit of the data for Cx45.6-56M1 (*dashed line*) is shown.

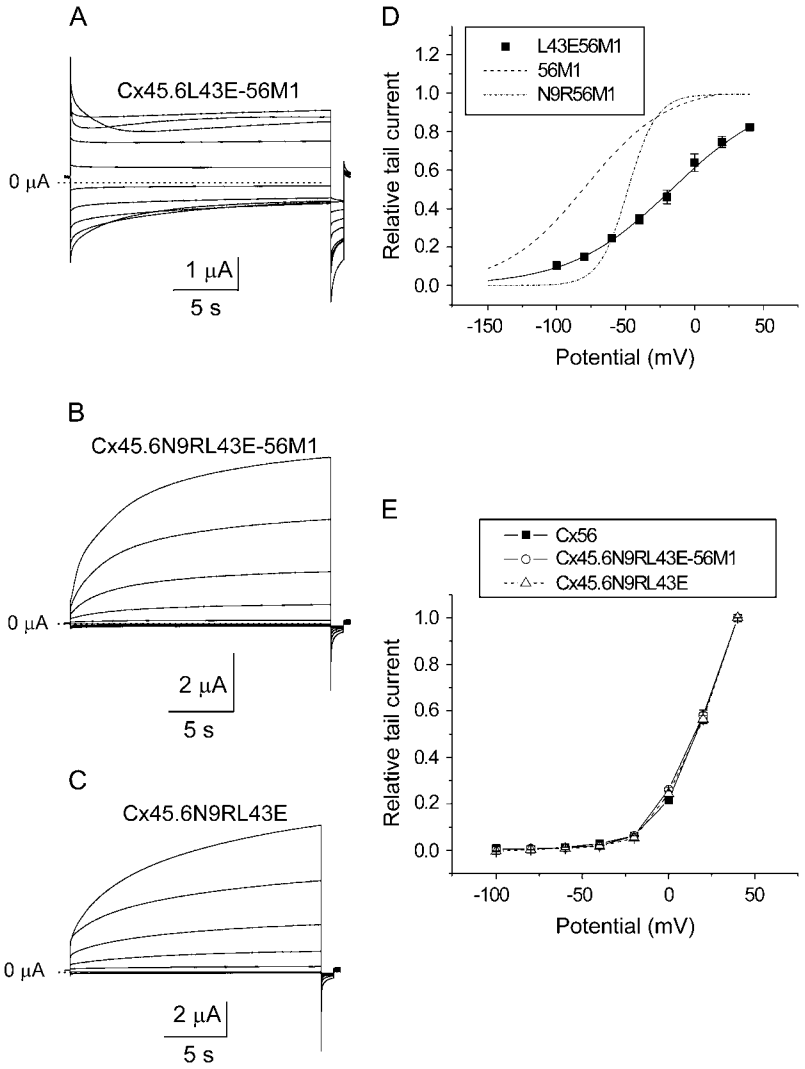

FIGURE 7 The voltage gating properties of Cx45.6N9RL43E-56M1 hemichannel currents strongly resemble those of wild-type chicken Cx56. (*A–C*) Representative families of current traces recorded from oocytes expressing Cx45.6L43E-56M1 (*A*), Cx45.6N9RL43E-56M1 (*B*), or Cx45.6N9RL43E (*C*) in the presence of zero added calcium. A series of voltage clamp steps were applied from +80 mV to −100 mV in 20-mV decrements from a holding potential of −10 mV. No leakage current correction. Dashed line represents zero current. (*D*) Normalized isochronal conductance-voltage curve for Cx45.6L43E-56M1 (*solid squares*, $n = 3$). Solid black line is the best fit of the data to a Boltzmann function whose parameters are given in Table 1. For comparison, the fits to the data for Cx45.6-56M1 (*long dash*) and Cx45.6N9R-56M1 (*short dash-dot*) line are shown. (*E*) Isochronal conductance-voltage curves for Cx56 (*solid squares*, $n = 3$), Cx45.6N9RL43E-56M1 (*open circles*, $n = 3$), and Cx45.6N9RL43E (*open triangles*, $n = 3$).

earthworm and was most likely due at least in part to accumulation and depletion of ions rather than a change in membrane conductance (19). Reintroduction of Mg^{2+} to the bathing solution caused a significant decrease in the magnitude of the current and restored voltage-dependent gating. A similar loss of voltage-dependent gating was observed for Cx45.6N9RL43E-56M1 and Cx56 channels after removal of external Mg^{2+}. In contrast, Cx45.6-56M1 channels which contain leucine instead of glutamic acid at position 43 were insensitive to external Mg^{2+}. The Cx45.6-56M1 channels remained open at large negative potentials and showed no pronounced voltage sensitivity even in the presence of 1 mM Mg^{2+}. These findings suggest that that E43 contributes to a binding site that mediates the effects of Mg^{2+} on gating.

Single channel conductance and rectification is altered by R9 and E43

To determine if the same amino acids that were responsible for the differences in gating were also responsible for the differences in single channel conductance, the single channel conductances of the various chimeras were measured in cell-attached patches (Table 2). Fig. 11 shows representative single channel I-V curves for Cx45.6-56M1, Cx45.6N9R-56M1, Cx45.6N9RL43E-56M1, and Cx56R9NE43L. The single channel I-V curve for Cx45.6-56M1 was linear with a slope conductance of 568 ± 19.8 pA ($n = 4$) at 0 mV, which is similar to the value of γ_0 of wild-type Cx45.6. Introduction of R9 into Cx45.6-56M1 caused the single channel I-V curve to become inwardly rectifying and reduced the slope conductance at 0 mV to 433 ± 9.01 pS. When both N9R and L43E were introduced into the chimera, there was a small further reduction in γ_o. However, this reduction was not statistically significant.

The single channel conductance of the reciprocal mutation, Cx56R9NE43L was also examined. Our data showed that when R9N and E43L were introduced into Cx56, γ_o increased to 527 ± 25.9 pS, which is similar to the value of γ_0 of wild-type Cx45.6 and the single channel I-V curve remained inwardly rectifying.

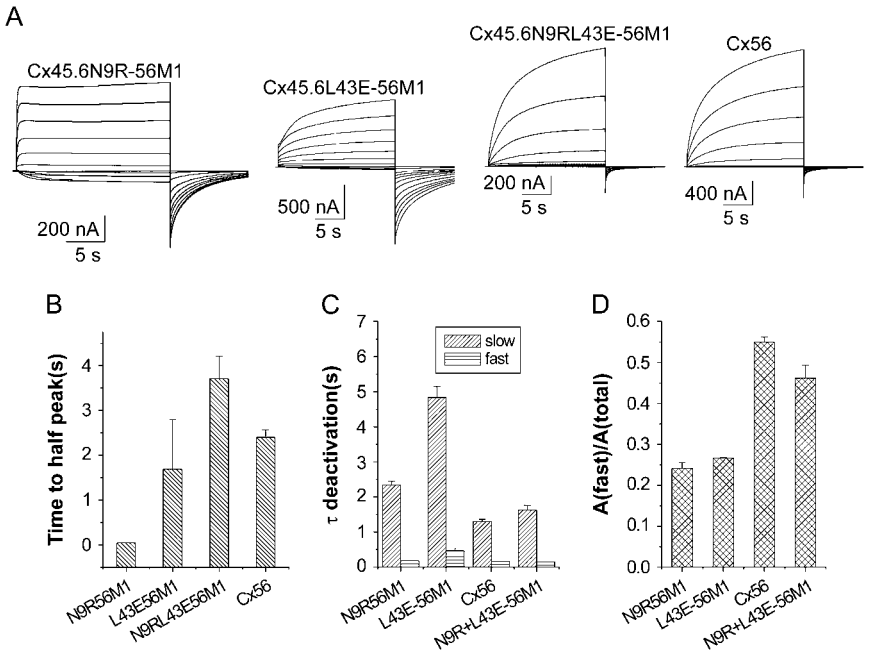

FIGURE 8 Activation and deactivation properties of Cx45.6N9R-56M1, Cx45.6L43E-56M1, Cx45.6N9RL43E-56M1, and wild-type chicken Cx56 hemichannel currents. (*A*) Representative families of current traces recorded from oocytes expressing chimeric and wild-type connexins. A series of voltage clamp steps were applied between −70 and +30 mV in increments of 10 mV from a holding potential of −80 mV in the presence of zero added calcium. Corrected for leakage current. Dashed line indicates zero current. (*B*) Time to half-peak activation at +30 mV ($n = 2$–5). (*C*) Fast and slow time constants of deactivation at −80 mV ($n = 2$–5). (*D*) Relative contribution of the fast component to the overall time course of deactivation at −80 mV ($n = 2$–5).

DISCUSSION

The main results of this project are that 1), chicken Cx56 and chicken Cx45.6 hemichannels show marked differences in current magnitude, voltage gating properties, and single channel conductance; 2), the first transmembrane-spanning domain, M1, is an important determinant of macroscopic current magnitude; 3), two charged amino acids that are specific for the α3-group connexins (R9 in the N-terminus and E43 in the first extracellular loop) are major determinants for the difference in voltage-dependent gating between Cx45.6 and Cx56 hemichannels; and 4), R9 and E43 are also determinants of single hemichannel conductance and rectification. Below we discuss the effects of exchanging different regions of the connexins on the voltage gating properties and single channel conductance of the hemichannels in greater detail.

Role of the first transmembrane-spanning domain

The magnitude of the hemi-gap-junctional currents in oocytes expressing the Cx45.6-56M1 chimera was significantly

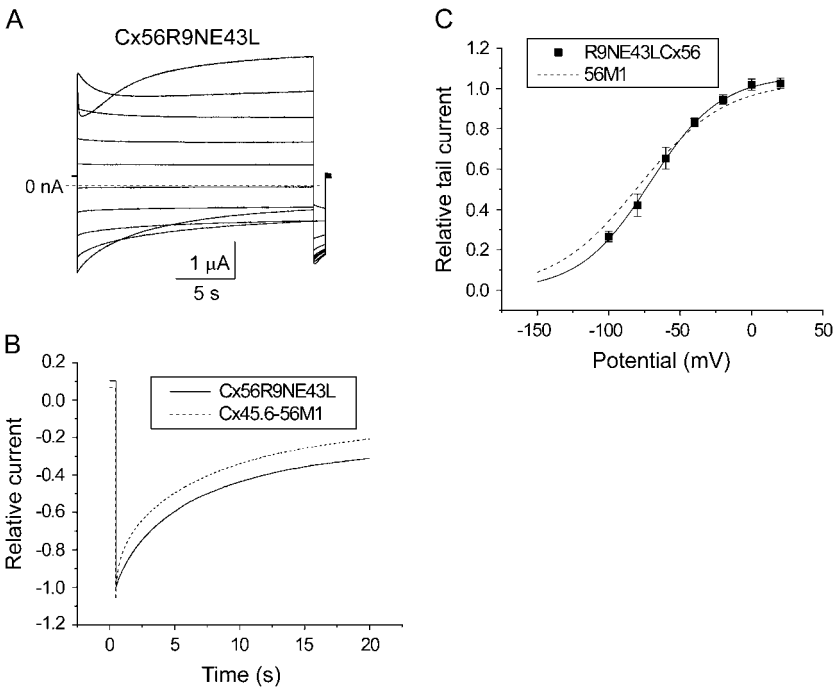

FIGURE 9 The reciprocal Cx56R9NE43L mutant exhibits a loss of rapid voltage-dependent gating at negative potentials. (*A*) Representative current traces recorded in response to a series of 20-s voltage clamp pulses from +80 mV to −100 mV in 20 mV decrements from a holding potential −10 mV in the presence of zero added calcium. Corrected by subtracting the average leakage current in control oocytes (oocytes injected only with AS). (*B*) Comparison of the time course of deactivation of Cx56R9NE43L and Cx45.6-56M1 currents on repolarization to −100 mV. The tail currents have been normalized with respect to the peak tail current. (*C*) Isochronal conductance-voltage curve for Cx56R9NE43L (*solid squares*, $n = 3$). Solid black line is the best fit of the data to a Boltzmann function whose parameters are given in Table 1. For comparison, the fit to the data for Cx45.6-56M1 (*long dash*) is shown.

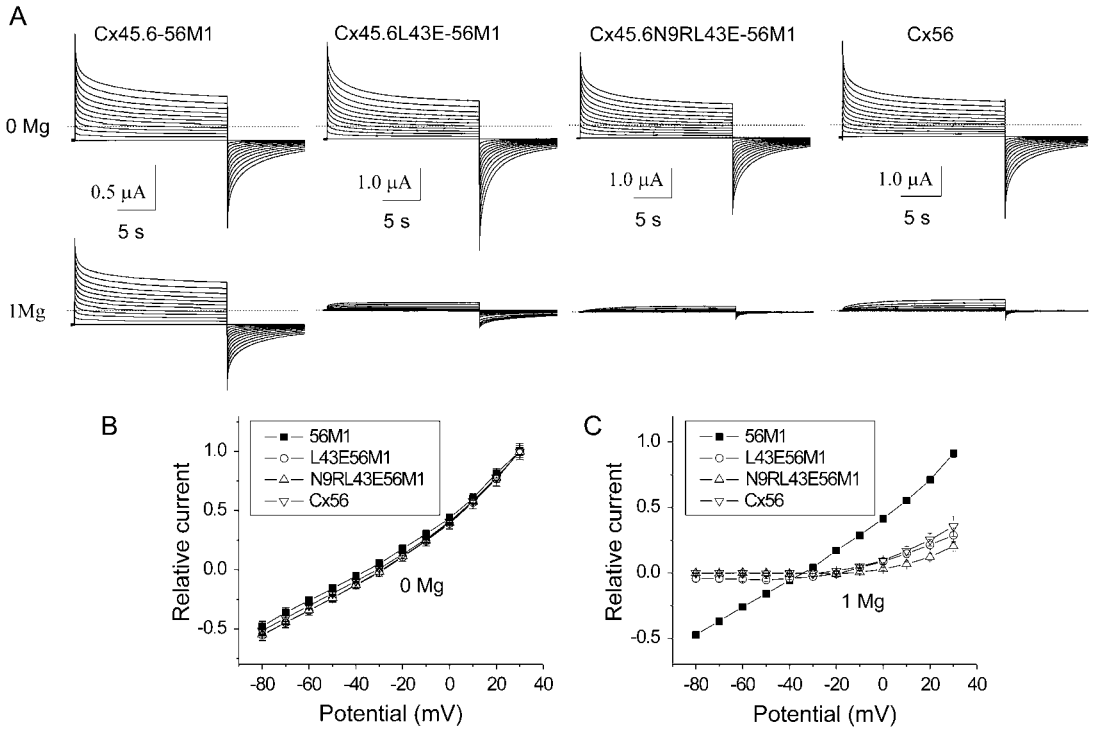

FIGURE 10 Effect of removal of Mg^{2+} on voltage-dependent gating of chimeric and wild-type channels. (*A*) Representative families of current traces recorded from oocytes expressing Cx45.6-56M1, Cx45.6L43E-56M1, Cx45.6N9RL43E-56M1, and Cx56 in the absence of Mg^{2+} (*upper panel*) and after wash-in of 1 mM Mg^{2+} (*lower panel*). A series of voltage clamp steps were applied between −70 and +30 mV in increments of 10 mV from a holding potential of −80 mV. Corrected for leakage. Dashed line indicates zero current. (*B* and *C*) Quasi-steady-state I-V relationships determined in the absence of external Mg^{2+} (*B*) and after wash-in of 1 mM Mg^{2+} (*C*).

larger than that recorded in oocytes injected with similar amounts of wild-type Cx45.6 cRNA. This increase in magnitude appeared to be due at least in part to a decrease in the blocking effect of external divalent cations on the hemichannel current. Swapping M1 had only minor effects on voltage-dependent gating of Cx45.6 hemichannels. Moreover, M1 did not appear to play an important role in determining single channel conductance and rectification. These results differ from those of Hu et al. (20,21), who found that important determinants for the differences in single channel conductance and gating of Cx46 and Cx32E(1)43 hemichannels were localized to the first transmembrane-spanning domain (M1) (20,21). These differences are most likely due to differences in the connexins used in these studies.

TABLE 2 Single channel conductances of wild-type and chimeric connexins

Cx	γ_o	Mean ± SE	No. of patches
Cx45.6	536.5	37.27488	4
Cx56	355.8	15.02091	6
Cx45.6-56M1	568.5*	19.84313	4
Cx45.6N9R-56M1	433	9.00925	4
Cx45.6N9RL43E-56M1	359.8†	28.40845	5
Cx56R9NE43L	527*	25.8908	3

*$p > 0.4$ where p is the probability that the mean of the slope conductance is identical to Cx45.6.
†$p \geq 0.9$ where p is the probability that the mean of the slope conductance is identical to Cx56.

Comparison of the amino acid sequences of chicken Cx45.6's M1 with homologous sequences of other α8- and α3-group connexins reveals differences at two locations: I36 and T39 are present in all of the α8-group connexins. In contrast, α3-group connexins contain V36 and A39 in these respective positions. It is not clear how these residues alter the Ca^{2+} sensitivity. One possibility is that the hydroxyl group of the threonine residue at position 39 which previous studies suggest is pore lining (22) provides a dipole moment for stabilizing calcium in the outer mouth of the channel. A more complex structural alteration of the outer mouth of the pore cannot be ruled out.

The calcium dose-response curve for Cx45.6 hemichannels in choline chloride solutions resembled that reported for Cx50 in sodium-containing solutions (16,23) except that the IC_{50} for Cx45.6 was lower than that for Cx50. In contrast, the calcium dose-response curve for Cx45.6-56M1 closely resembled that of Cx46 measured in response to application of progressively increasing calcium concentrations (16). These results suggest that the decreased sensitivity to calcium block of Cx46 may be partially accounted for by differences in M1.

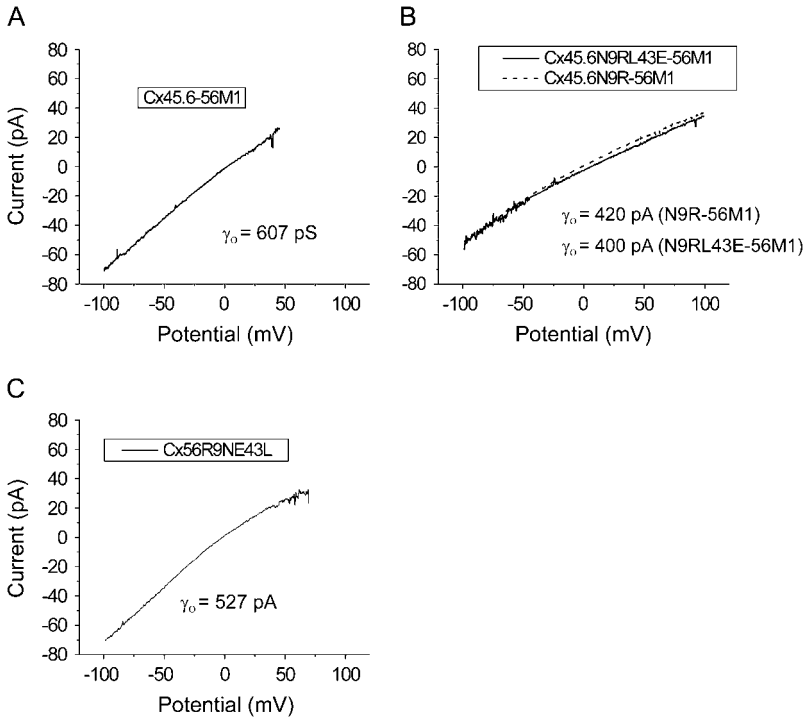

FIGURE 11 Single channel I-V curves of wild-type and chimeric connexins recorded in the cell-attached patch configuration using ±100-mV voltage ramps. Records were obtained with pipette and bath solutions composed of 140 mM KCl, .5 mM Ca^{2+}, 1 mM Mg^{2+}, 1 mM EGTA, pH 7.6. Corrected for leakage currents as described in Materials and Methods.

Role of the N-terminal

There is good evidence that the first 11–12 amino acids of the N-terminus of connexin Cx32 and other β-group connexins reside within the channel pore when the channel is open and acts as the voltage sensor for V_j-gating (24–27). Several recent studies suggest that the N-terminus may play a similar role for the α-group connexins (17,18,28).

In this study, we show that replacement of the N-terminal region of Cx45.6 with the corresponding domain of Cx56 resulted in fast channel closure when the membrane potential was changed to negative potentials. Further experiments showed that the positive charge at residue 9 was the main determinant for this effect. This amino acid is completely conserved in all of the α3-group connexins and is absent in all of the α8-group connexins supporting its central role in determining the voltage gating properties of the α3-group hemichannels.

How addition of a positive charge at residue 9 produces rapid voltage gating at negative potentials is unknown. One possibility is that R9 resides within the pore when the channel is open. Application of a negative transmembrane potential displaces R9 by electrostatic attraction to negative intracellular voltage. This in turn causes the channel to close. Alternatively, external divalent cations could enter the channel and bind to a nearby site, thus displacing R9 by electrostatic repulsion. Evidence for the second hypothesis comes from the observation that removal of all external divalent cations causes a marked slowing of deactivation (data not shown).

In addition to its role in voltage gating, our results show that R9 is an important determinant of single channel conductance and rectification. When R9 was introduced into Cx45.6-56M1, the single channel I-V curve became inwardly rectifying and the slope conductance at 0 mV decreased to a value that more closely resembled that of wild-type Cx56. These findings are consistent with the results of a previous study which identified R9 as the main determinant for the differences in single channel conductance observed between Cx45.6 and Cx56 gap junctional channels (18) and provide further evidence for the hypothesis that R9 contributes to the pore lining.

Role of E43

The other critical amino acid is E43. This residue is located near the beginning of the first extracellular domain, E1. It is present in most of the α3-group connexins, including Cx56, and is absent in all of the α8-group connexins. Cysteine scanning mutagenesis experiments suggest that this amino acid contributes to the pore lining region of α3-group hemichannels (22). Previous studies on other connexins such as Cx32 and Cx26 have implicated this amino acid in the voltage gating of gap junctional channels (24,25,29).

In this study, we show that the introduction of E43 into Cx45.6-56M1 caused the channel to close at large negative potentials in a time- and voltage-dependent manner and slowly reopen upon depolarization. In the absence of magnesium, however, the channel remained predominantly in the open state even at large, negative potentials and showed no pronounced voltage sensitivity. The simplest explanation for these findings is that the L43E mutation is contributing to a

divalent cation binding site within the membrane field that binds Mg^{2+} and thereby causes voltage-dependent closure at large negative potentials. Upon depolarization, magnesium slowly unbinds, resulting in channel opening. A similar model has been proposed to account for the voltage gating properties of Cx37 hemichannels (12).

When E43 was combined with R9, it shifted the threshold of activation by ~+40 mV compared to Cx45.6N9R-56M1, slowed the time course of activation, and accelerated the time course of deactivation. The voltage gating properties of the Cx45.6N9RL43E-56M1 chimera displayed a remarkable resemblance to those of wild-type Cx56. The importance of R9 and E43 in determining the voltage-dependent gating properties of Cx56 hemichannels was further supported by the finding that introduction of the reciprocal point mutations (R9N and E43L) into wild-type Cx56 converted many biophysical properties of the resulting mutant channel back to those of Cx45.6-56M1. Similar to Cx45.6L43E-56M1, the gating of Cx45.6N9RL43E-56M1 and Cx56 channels required the presence of external divalent cations. One possible explanation for the increased stability of the double point mutant (Cx45.6N9RL43E-56M1) in the closed state at negative potentials is that the binding of one or more magnesium ions to the divalent cation binding site contributed by E43 causes a conformational change in the channel that displaces R9 from the channel pore, resulting in channel closure. Alternatively, the presence of E43 might influence gating by acting as an accessory divalent cation binding site that increases the concentration of divalent cations near or within the pore as has been previously proposed by Puljung et al. (12) to account for the discrepancy in time course of closure of Cx37 hemichannels under different experimental conditions. Further experimentation and structural information will be needed to better elucidate these interactions.

SUMMARY

The gating mechanism that closes Cx56 hemichannels at negative potentials in a divalent cation- and voltage-dependent manner corresponds to the so-called ''loop gating'' mechanism identified by Trexler et al. (30). This gate is largely absent in Cx45.6 and other α8-group connexins (16,17). Our results demonstrate that R9 in the N-terminus, which has been previously shown to play an important role in the transjunctional voltage gating of α3 gap junctional channels, also plays an important role in the voltage- and divalent cation-dependent gating of Cx56 hemichannels at negative potentials. In addition, the results indicate that E43 in the first extracellular loop plays a crucial role in this process.

The voltage- and divalent cation-dependent gating mechanism of Cx56 is designed to keep Cx56 hemichannels closed at negative potentials but allow them to open on depolarization in the presence of physiological external divalent cation concentrations. In contrast, Cx45.6 hemichannels always remain in the closed state. These differences in gating properties might be of physiological relevance. It has been suggested in the literature that hemichannels may play a role in visual accommodation or in the generation of circulating ionic fluxes in the lens (3,16).

This study was supported by National Institutes of Health grant EY10589.

REFERENCES

1. John, S. A., R. Kondo, S.-Y. Wang, J. I. Goldhaber, and J. N. Weiss. 1999. Connexin-43 hemichannels opened by metabolic inhibition. *J. Biol. Chem.* 274:236–240.
2. Contreras, J. E., H. A. Sanchez, E. A. Eugenin, D. Speidel, M. Thiels, K. Willecke, F. F. Bukauskas, M. V. Bennett, and J. C. Saez. 2002. Metabolic inhibition induces opening of unapposed connexin 43 gap junction hemichannels and reduces gap junctional communication in cortical astrocytes in culture. *Proc. Natl. Acad. Sci. USA.* 99: 495–500.
3. Bao, L., and F. Sachs. 2004. Connexins are mechanosensitive. *Am. J. Physiol.* 287:C1389–C1395.
4. Cotrina, M. L., J. H.-C. Lin, A. Alves-Rodrigues, S. Liu, J. Li, H. Azmi-Ghadmimi, J. Kang, C. C. G. Naus, and M. Nedergaard. 1998. Connexins regulate calcium signaling by controlling ATP release. *Proc. Natl. Acad. Sci. USA.* 95:15735–15740.
5. Stout, C. E., J. L. Costantin, C. C. G. Naus, and A. C. Charles. 2002. Intercellular calcium signaling in astrocytes via ATP release through connexin hemichannels. *J. Biol. Chem.* 277:10482–10488.
6. Bruzzone, S., L. Guida, E. Zocchi, L. Franco, and A. De Flora. 2001. Connexin 43 hemichannels mediate Ca2+-regulated transmembrane NAD+ fluxes in intact cells. *FASEB J.* 15:10–12.
7. Leybaert, L., K. Braet, W. Vandamme, L. Cabooter, P. E. Martin, and W. H. Evans. 2003. Connexin channels, connexin mimetic peptides and ATP release. *Cell Commun. Adhes.* 10:251–257.
8. Willecke, K., J. Eiberger, J. Degen, D. Eckardt, A. Romualdi, M. Guldenagel, U. Deutsch, and G. Sohl. 2002. Structural and functional diversity of connexin genes in the mouse and human genome. *Biol. Chem.* 383:725–737.
9. DeVries, S. H., and E. A. Schwartz. 1992. Hemi-gap-junction channels in solitary horizontal cells of the catfish retina. *J. Physiol.* 445:201–230.
10. Pfahnl, A., and G. Dahl. 1999. Gating of Cx46 gap junction hemichannels by calcium and voltage. *Pflugers Arch.* 437:345–353.
11. Gomez-Hernandez, J. M., M. de Miguel, B. Larrosa, D. Gonzalez, and L. C. Barrio. 2003. Molecular basis of calcium regulation in connexin-32 hemichannels. *Proc. Natl. Acad. Sci. USA.* 100:16030–16035.
12. Puljung, M. C., V. M. Berthoud, E. C. Beyer, and D. A. Hanck. 2004. Polyvalent cations constitute the voltage gating particle in human connexin37 hemichannels. *J. Gen. Physiol.* 124:587–603.
13. Ebihara, L., and E. Steiner. 1993. Properties of a nonjunctional current expressed from a rat connexin46 cDNA in Xenopus oocytes. *J. Gen. Physiol.* 102:59–74.
14. Ebihara, L. 1996. Xenopus Connexin38 forms hemi-gap-junctional channels in the nonjunctional plasma membrane of Xenopus oocytes. *Biophys. J.* 71:742–748.
15. Methfessel, C., V. Witzemann, T. Takahashi, M. Mishina, S. Numa, and B. Sakmann. 1986. Patch clamp measurements on *Xenopus laevis* oocytes: currents through endogenous channels and implanted acetylcholine receptor and sodium channels. *Pflugers Arch.* 407:577–588.
16. Beahm, D. L., and J. E. Hall. 2002. Hemichannel and junctional properties of connexin 50. *Biophys. J.* 82:2016–2031.

17. Srinivas, M., J. Kronengold, F. F. Bukauskas, T. Bargiello, and V. Verselis. 2005. Correlative studies of gating in Cx46 and Cx50 hemichannels and gap junction channels. *Biophys. J.* 88:1725–1739.

18. Tong, J. J., X. Liu, L. Dong, and L. Ebihara. 2004. Exchange of gating properties between rat Cx46 and chicken Cx45.6. *Biophys. J.* 87:2397–2406.

19. Brink, P. R., R. T. Mathias, S. W. Jaslove, and G. J. Balso. 1988. Steady-state current flow through gap junctions. *Biophys. J.* 53:795–807.

20. Hu, X., and G. Dahl. 1999. Exchange of conductance and gating properties between gap junction hemichannels. *FEBS Lett.* 451:113–117.

21. Hu, X., M. Ma, and G. Dahl. 2006. Conductance of connexin hemichannels segregates with the first transmembrane segment. *Biophys. J.* 90:140–150.

22. Kronengold, J., E. B. Trexler, F. F. Bukauskas, T. A. Bargiello, and V. K. Verselis. 2003. Single-channel SCAM identifies pore-lining residues in the first extracellular loop and first transmembrane domains of Cx46 hemichannels. *J. Gen. Physiol.* 122:389–405.

23. Srinivas, M., A. C. Campos de Carvalho, J. Kronengold, and V. Verselis. 2006. Regulation of connexin hemichannels by monovalent cations. *J. Gen. Physiol.* 127:67–75.

24. Verselis, V. K., C. S. Ginter, and T. A. Bargiello. 1994. Opposite voltage gating polarities of two closely related connexins. *Nature*. 368:348–351.

25. Oh, S., C. K. Abrams, V. K. Verselis, and T. A. Bargiello. 2000. Stoichiometry of transjunctional voltage-gating polarity reversal by a negative charge substitution in the amino terminus of a connexin32 chimera. *J. Gen. Physiol.* 116:13–31.

26. Purnick, P. E., S. Oh, C. K. Abrams, V. K. Verselis, and T. A. Bargiello. 2000. Reversal of the gating polarity of gap junctions by negative charge substitutions in the N-terminus of connexin 32. *Biophys. J.* 79:2403–2415.

27. Purnick, P. E., D. C. Benjamin, V. K. Verselis, T. A. Bargiello, and T. L. Dowd. 2000. Structure of the amino terminus of a gap junction protein. *Arch. Biochem. Biophys.* 381:181–190.

28. Musa, H., E. Fenn, M. Crye, J. Gemel, E. C. Beyer, and R. D. Veenstra. 2004. Amino terminal glutamate residues confer spermine sensitivity and affect voltage gating and channel conductance of rat connexin40 gap junctions. *J. Physiol.* 557:863–878.

29. Rubin, J. B., V. K. Verselis, M. V. Bennett, and T. A. Bargiello. 1992. A domain substitution procedure and its use to analyze voltage dependence of homotypic gap junctions formed by connexins 26 and 32. *Proc. Natl. Acad. Sci. USA.* 89:3820–3824.

30. Trexler, E. B., M. V. Bennett, T. A. Bargiello, and V. K. Verselis. 1996. Voltage gating and permeation in a gap junction hemichannel. *Proc. Natl. Acad. Sci. USA.* 93:5836–5841.